Robust Active Learning Multiple Fault Diagnosis of Sensorless PMSM Drives in Dynamic Operations Under Imbalanced Datasets

Sveinung Attestog, Jagath Sri Lal Senanayaka, Huynh Van Khang, Kjell G. Robbersmyr

This paper has been published as:

S. Attestog, J. S. L. Senanayaka, H. Van Khang, and K. G. Robbersmyr, "Robust Active Learning Multiple Fault Diagnosis of Sensorless PMSM Drives in Dynamic Operations Under Imbalanced Datasets", IEEE Transactions on Industrial Informatics (under revision).

F.1 Abstract

This paper proposes an active learning scheme to detect multiple faults in permanent magnet synchronous motors in dynamic operations without using historical labelled faulty training data. The proposed method combines the self-supervised anomaly detector based on local outlier factor (LOF) and a deep Q-network (DQN) supervised reinforcement learner to classify inter-turn short-circuit, local demagnetisation and mixed faults. The first fault, which is detected by LOF and verified by an expert during maintenance, is used as training data for the DQN classifier. From that point onward, LOF anomaly detector and DQN fault classifiers are working in tandem in identification of new faults, which require an expert intervention when either of them identifies a fault. The robustness of the scheme against dynamic operations, mixed fault and imbalanced training datasets is validated via a comparative study using stray flux data from an in-house test setup.

F.2 Introduction

Permanent magnet synchronous motors (PMSM) in off-shore wind turbines and electric vehicles are intensively exposed to mechanical and thermal stresses in dynamic operations with thermal cycling. These result in inter-turn short-circuit (ITSC), and local demagnetisation fault (DF) [1]. A local demagnetisation only affects a small region of rotor magnets in early states, and induces a magnetic asymmetry in contrast to uniform DF, which downgrade all magnets equally. Detecting and identifying these faults in incipient stages allow for life prolonging operation or planned maintenance, reducing costs and production down-times [2]–[4].

Fault detection and identification (FDI) methods for electrical machines have been extensively developed and categorised as: model-, signal- and machine learning (ML) based methods [5]. The model-based methods aim to identify fault signatures by estimating hard-to-measure parameters and computing a residual between a suggested model and measurements. This approach relies on the accurate information of physical parameters in the model or detailed dimensions of machines, which are difficult to acquire in reality [6]. Signal processing methods detect a fault based on fault-related characteristic frequencies. These methods are simple but are only applicable to single fault diagnosis. Further, missing a fault characteristic frequency does not guarantee that a machine is completely healthy. ML based methods have recently gained popularity since they are less demanding on prior knowledge of a machine [7].

To address the lack of labelled faulty data issues, anomaly detection has been used in various studies [8], [9]. These anomaly detectors and one-class classifiers (OCCs) train on the observation from the healthy cases. A trained OCC can quantify the deviation of a new data sample from the healthy samples. A large deviation from a healthy sample is considered as a faulty case. Krawczyk et. al. [10] separate the OCCs into four categories namely; (1) Density-based methods e.g. local outlier factor (LOF) [11], (2) Reconstruction-based methods such as auto-encoder [12] and contrastive learning [13], (3) Boundary-based methods e.g., one-class SVM [8], (4) Ensemble-based methods which combine OCCs to form a more flexible data description model [10]. It is important to

use a proper comparative study to find the best OCC type for a given anomaly detection application. However,to the authors' knowledge, finding the best OCC method for detecting anomaly in PMSMs has not been studied in the literature.

Another method to tackle the lack of labelled faulty data is using active learning (AL). It is a set of semi-supervised learners [14], [15], which are used to accelerate the labelling process of partially labelled dataset. They are trained on the labelled samples and tests on the unlabelled samples. The prediction with the lowest confidence is passed to an expert, who "actively" labels the dataset for the ML-based detection. An AL is often called a cooperative learner when it significantly alleviates the labelling task for the expert. Alternatively, a self-supervised anomaly detector can be implemented in an AL scheme. Senananyaka et. al. [8] proposed a FDI development scheme without using historical data from operating faulty motors. Within the study, a self-supervised one-class SVM is first used to detect the anomaly. However, this OCC defines healthy domain based on its kernel function and may include regions of low competence. It will have a high rate of false negatives (FN) if the healthy and faulty classes overlap. The second part of the presented FDI scheme is a convolutional neural network (CNN) classifier, which is trained by samples identified by the one-class SVM and validated by an expert. Further development of such a FDI will create a more competent CNN with knowledge of faults, that have occurred. The authors in [8] trained and tested the FDI scheme on a balanced dataset alone. However, obtaining a balanced dataset for ML-based fault diagnosis methods is not feasible from PMSMs in offshore wind turbines. Developing a novel fault diagnosis must take the imbalance in datasets into consideration.

Imbalance in a dataset is often measured by the ratio (λ) between negative (healthy) and positive (faulty) samples. The problem of imbalance data set is amplified due to noise, overlap between classes, and if one class is represented by multiple clusters [16]. A common method for "rebalancing" the imbalanced data set is to oversample the minority class and undersample the majority class. Both of these processes can be executed by random sampling. However, the minority class also has an option for generating new synthetic samples with different variations of synthetic minority oversampling technique (SMOTE) or extraction maximisation imputation-based class imbalanced learning [17]. Zhang et. al. [12] proposed a self-supervised feature learning scheme for bearing fault in steady state with less than 50 labelled training samples per class. A CNN is trained with augmented data to match the computed pseudo labels, which consist of statistical features and features extracted from an auto-encoder. This allows for rich feature mining from a small number of positive samples. However, the existing studies could deal with imbalanced datasets for detecting single faults alone in steady states while using a lot of historical data at faulty conditions.

This study aims to develop a novel scheme of mixed fault diagnosis in sensorless PMSM drives under dynamic operations while addressing the problems of imbalanced datasets using limited samples from faulty conditions. Within the framework, an anomaly detector is developed based on a LOF to define more complex domains in healthy cases to tackle overlapping classes. The proposed scheme is proven to be robust against dynamic operations at different operation profiles by resampling at a fixed angular increment without using any position sensor. This suggested scheme, using external flux sensors alone, allows

for developing a plug-and-play automatic fault detection without modifying the existing drive systems in critical or offshore applications, where sensorless controls are preferred due to reliability or reduced maintenance cost.

F.3 Proposed Fault Diagnosis Scheme

The proposed FDI scheme shown in Figure F.1 is developed based on an online fault diagnosis scheme in [8]. The pretreatment after data collections involves resampling of the original time-series data at a fixed angular increment. The rotor position is estimated from one stray flux measurement with an optimisation problem, being detailed in Section III. The resampled data is split into intervals of 30 revolutions, which are converted to the frequency domain by fast-Fourier transform (FFT). The spectrograms are normalised with respect to both amplitude and frequency of the fundamental component. Then, the spectrograms are enveloped by splitting the spectrogram into intervals with a length of 0.5 order centred around the half harmonics (0.5, 1, 1.5, ...) to find the maximum in each interval. This saves the storage space while maintaining the information on the half harmonics. The pretreatment makes the FDI scheme robust against transient operation condition and can be implemented in sensorless drives.

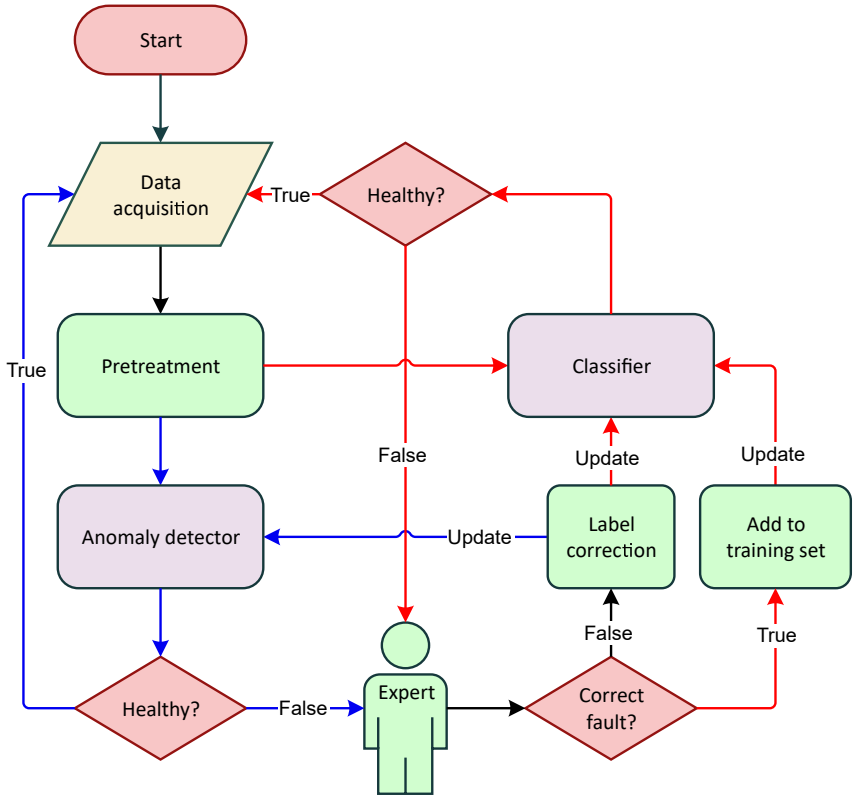

Figure F.1: Flowchart of the proposed FDI scheme. Note: Arrows coloured in red, blue and black represent information flow related to classifier, detector or both; Green objects represent processes/actions; purple boxes represent detector and classifier, red diamonds represent decisions

The FDI scheme starts with detecting anomaly using a self-supervised anomaly de-

tector, since historical data at faulty is not available. If the anomaly detector gives a false positive (FP), which is determined by an expert, it then needs to be updated with these FPs to learn the new region of healthy case. True positive samples marks the end of the first stage of the FDI scheme since the samples of faulty case are now available for training of the fault classifier. The second stage keeps the fault detector, but it works alongside with the fault classifier. An investigation by an expert is required when either the detector or classifier identifies a fault. If a fault is detected and classified as a previously discovered fault, the fault search can be narrowed down during maintenance. Note that in the first iteration of stage 2, the classifier only knows of one fault. However, more data during operations will result in a more knowledgeable and confident FDI, which can speed up the maintenance process, reducing unexpected downtime and cost. The detailed description of the FDI is given in Algorithm 1.

Algorithm 1 Detailed description of FDI scheme

```
Require: Healthy case data set, threshold, maintenance expert
  while No discovered faulty cases do
      Compute Anomaly score with OCC
      if Anomaly criterion = TRUE then:
          Expert investigation
          if Fault = TRUE then:
              Perform maintenance
              Label newly discovered fault and train classifier
          else if Fault = FALSE then
              Update OCC
          end if
      end if
  end while
  while At least one discovered fault class do
      Compute Anomaly score with OCC
      Predict fault class with classifier
      if A fault is detected by classifer or OCC then:
          Expert investigation
          if Fault = TRUE then:
              Perform maintenance
              if Fault = New then
                  Label new fault and update classifier
              else if Fault = Old then
                  Label new fault samples and update classifier
              end if
          else if Fault = FALSE then
              Updata OCC
          end if
      end if
  end while
```

F.3.1 Anomaly detection

The existing anomaly detectors using self-supervised learners need samples from healthy cases to identify any anomalies, which later can be labelled by an expert for initiating the training of a fault classifier in a later stage. The suggested one-class SVM in [8] is replicated, and 10 % of the training data is assumed to be outliers. The drawback with this OCC is its assumption of defining the region of healthy case with the kernal function. Regions of low competence may be included to increase the chance of FN. To address this demerit, a density based method LOF in [11] is used in this work to replace the one-class SVM. Like the k-nearest neighbours, the pair-wise distance between all the samples in the training dataset needs to be computed. This will make the LOF computationally heavy when the library of samples in the healthy case become too large. This problem can be solved by selective samplings [18].

The samples in datasets are grouped into clusters. An outlier can be isolated by a threshold value of the average distance to its nearest neighbours. However, the samples of the healthy dataset do not necessarily have a uniform density in its cluster in feature space. Thus anomalies can be closer to a cluster, depending on the region in the feature space [11]. LOF isolates outliers based on the sample density $\rho_{\mathbf{samp}}$ in feature space.

$$\rho_{\text{samp}}(P) = \left(\frac{1}{k} \sum_{n=1}^{k} d(P, o_n) \right)^{-1} \tag{F.1}$$

where k is an integer, $d(P, o_n)$ is the pair-wise Euclidean distance between point P and its nearest neighbours o_n. Then the sample density of each of the neighbour points o_n ($\rho_{\text{samp}}(o_n)$) needs to be computed. LOF is here defined as:

$$\text{LOF}(P) = \frac{1}{k} \sum_{n=1}^{k} \frac{\rho_{\text{samp}}(o_n)}{\rho_{\text{samp}}(P)} \tag{F.2}$$

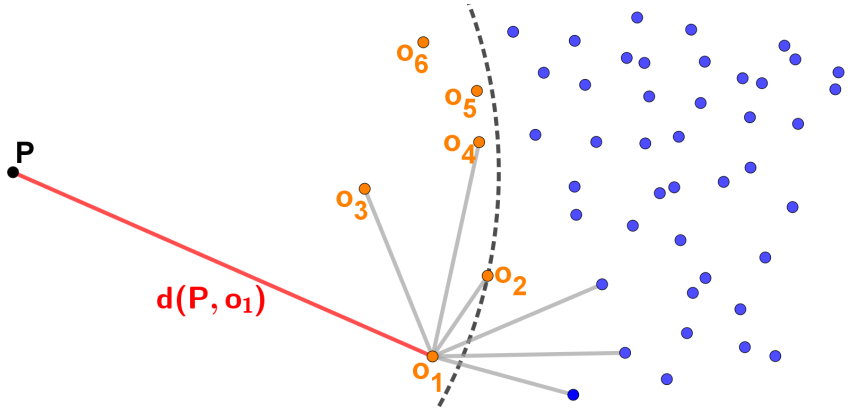

Figure F.2: Illustration of LOF in a 2D-feature space with P (black), o_n (orange), $d(P, o_1)$ (red), distance between o_1 to its nearest neighbours (gray), and rest of samples in the cluster (blue)

Figure F.2 illustrates the principle of LOF. The sixth nearest neighbours for point P are coloured in orange, while the rest of the dataset is coloured in blue. Point o_1 is

used as an example, where o_1 and its sixth nearest neighbours have grey connections. An anomaly is detected if LOF is greater than a set threshold. This implies that the new observation P is located in a region, which is a too "sparsely" populated region in feature space.

F.3.2 Fault identification

After the anomaly detection, the multiple fault identifications are implemented by a reinforcement learning (RL) based classifier in this study. RL has already proven its effectiveness in information theory, simulation-based optimisation, control theory and statistics [19], [20] and developed for bearing fault diagnosis alone [21] while the imbalance issues were not addressed. The proposed RL scheme based on a double deep Q-network (DQN) in [22] will be compared with the recently developed using a CNN architecture for fault identification in [8]. The problem with the existing CNN classifier is that it is not suited for imbalance datasets. The proposed DQN fault classifier can compensate the imbalance datasets without any oversampling. RL usually uses the analogy of teaching the agent to play a game. In the fault classification, the RL agent plays a "quiz game". It is formulated in form of 1D arrays as features, where the agent needs to give a response on classification. The Q-learning aims to set up a Q-table that contains the policy to maximise a reward depending on the input. In DQN, the Q-table is replaced with a neural network. Figure F.3 illustrates the interaction between the DQN agent and its environment. The illustration inside the DQN shows the layers of the critic network with four layer: Input layer (243 nodes), fully connected layer (100 nodes), ReLU activation function layer and the second fully-connected layer. The number of nodes in the final layers is equal to number classes in the training data.

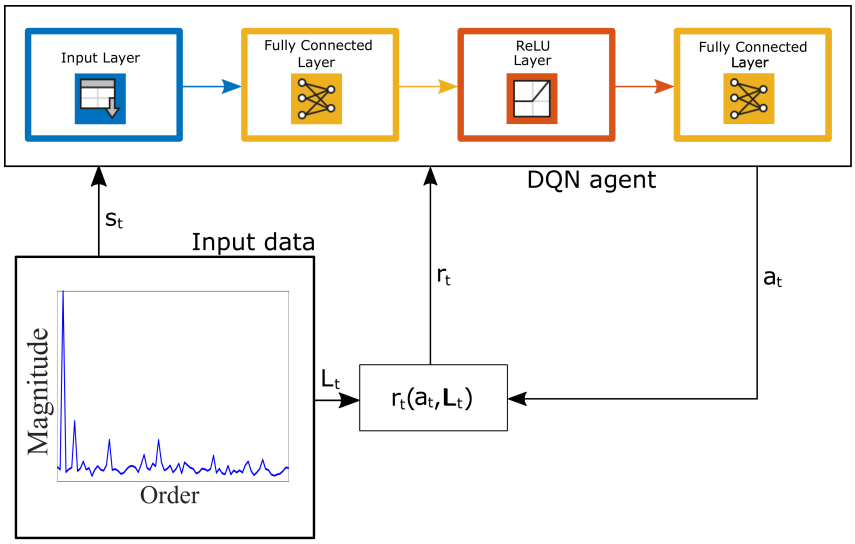

Figure F.3: Block diagram of DQN interacting with the environment

The action of the agent is associated with the label of the training dataset. If there is only two classes in the training set, it is sufficient to define the action space as $A = \{0, 1\}$. In this study, the action space is defined as $A = \{[0, 0], [0, 1], [1, 0], [1, 1]\}$. The entries in

A represent healthy or no fault (NF), DF, ITSC and mixed fault (MF), respectively. MF is the mix of DF and ITSC. The encoding of the labels is for the DQN only, which needs to be decoded after the prediction.

The reward function [22] is weighted based on the ratio between negative (healthy case) and positive (faulty case) samples.

$$r_t = \begin{cases} 1, & a_t = L_t = \text{Healthy} \\ -1, & a_t \neq L_t = \text{Healthy} \\ \lambda, & a_t = L_t = \text{Faulty} \\ -\lambda, & a_t \neq L_t = \text{Faulty} \end{cases} \tag{F.3}$$

The performance of a classifier to identify positive samples will decline when the imbalance ratio λ is increased. Eventually, the network will classify every sample as negative regardless of input. This phenomenon is called a collapse and is caused by the fact that the negative samples receive a greater sway in the training of the network since they are in majority. The role of r_t is to tackle the trend towards a collapse by balancing the weights of the negative and positive samples in the training process. The training process of the DQN is described in Algorithm 2 [23], where Θ is the parameter critic and τ is the smoothing factor for updating the target critic, which has the parameter Θ_t. There is no terminal state for S_{t+1}.

Algorithm 2 Training Algorithm for DQN

Require: Positive and negative samples
  for N_{epi} episode **do**
    Pick a random sample s_1 from the training set
    for N_{step}-1 steps **do**
      if Exploration **then**
        Pick a random action a_t from A
      else
        $a_t = \max_{a_t} = Q(s_t, a_t|\Theta)$
      end if
      Execute a_t and observe the reward r_t
      Randomly pick s_{t+1} from training set
      Store the experience (s_t, a_t, r_t, s_{t+1})
      Compute and store the value function:
      $y_t = r_t + \gamma \arg\max_{a_t} Q_t(s_{t+1}, a_{t+1}|\Theta_t)$.
      Compute the loss for a mini-batch with M samples:
      $L = \frac{1}{M}\sum_{t=1}^{M}\left(y_t - Q(s_t, a_t|\Theta)\right)^2$
      Update the critic by one-step minimisation
      Update the target critic parameters: $\Theta_t = \tau\Theta + (1-\tau)\Theta$
      Update the decaying probability for exploration
      Repeat
    end for
  end for

F.4 Experimental setup and data collection

F.4.1 In-house test bench

The studied four-pole, 2.2 kW PMSM is coupled to a generator with a torque transducer in between as shown in Figure F.4. The output of the generator is rectified by a three-phase full-bridge rectifier with a 500 μF capacitor bank, being connected across the output terminals, to remove the ripples of the DC output. The brake chopper is regulated by a PWM signal, which needs to be amplified by a factor of 4 due to the voltage amplitude insufficiency from the Microlabbox. The PWM signal is defined by the duty cycle, which is an ideal system that would be proportional to the reciprocal of the motor speed. However, due to losses and imperfections, a look-up table is generated for the duty cycle. It dictates the required duty cycle for achieving a requested load in the speed range between 1000 rpm and 2000 rpm.

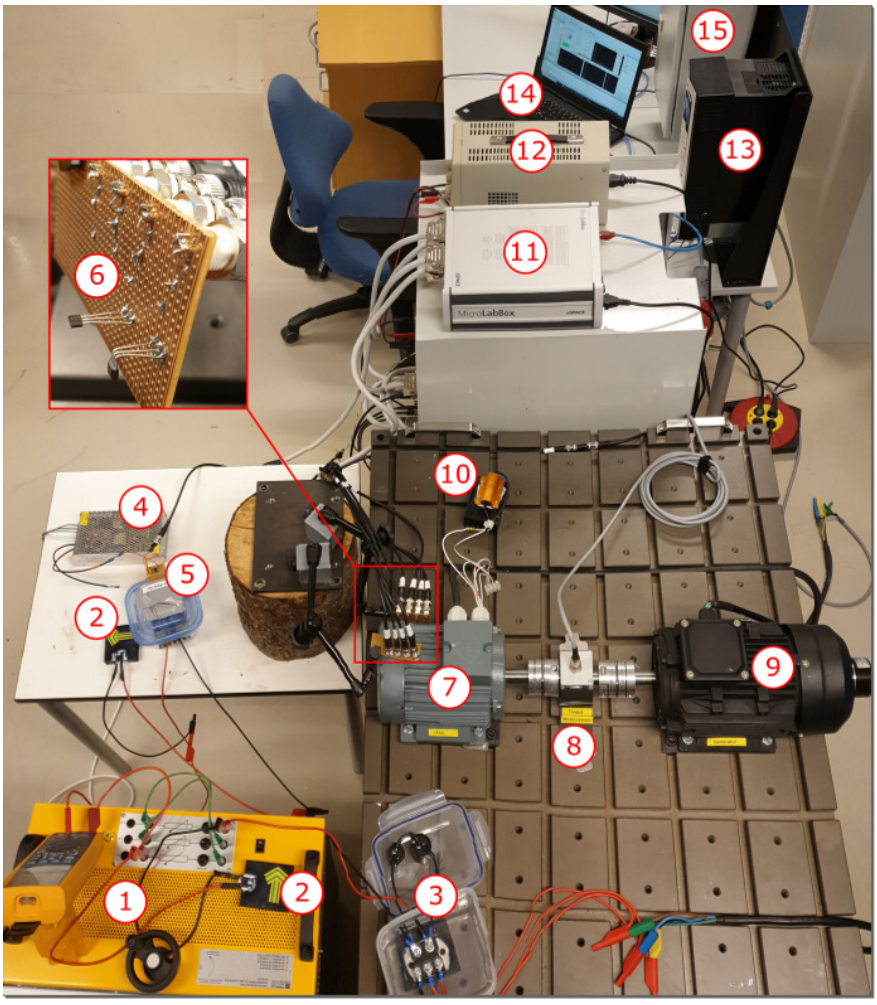

Figure F.4: Overview of the test bench with (1) resistor bank, (2) flyback diode, (3) three-phase rectifier with capacitor bank, (4) 12 V DC-supply, (5) IGBT brake chopper with OP-Amp, (6) hall sensors, (7) PMSM, (8) torque transducer, (9) generator, (10) short circuit resistor, (11) Microlabbox, (12) 24 V DC-supply, (13) ABB drive, (14) office laptop and (15) cabinet containing the current sensors

The solid state hall sensors, Type SS495A, measure the stray flux. The output of these sensors is linear and ratio-metric within the range [-67, 67] mT and has a sensitivity of 31.25 $\frac{mV}{mT}$. Two sensors were soldered to a Veroboard and wired to the Microlabbox, which delivers power to the sensors and records the measurement. The sensors could measure both tangential and radial components of the stray flux. Two sets of sensors were placed in proximity to the PMSM at the top and on the side.

F.4.2 Description of collected datasets

Stray fluxes are measured for three different non-stationary operating conditions with a sampling rate of 10 kHz. The time-series data is resampled with 400 samples per rotor revolution and split into samples with a length of 30 revolutions. Each sample is transformed into the frequency domain to produce the features for each observation used for training and testing of the proposed algorithm. The test setup is operated with the the three operation profiles shown in Figure F.5. Profile 1 consists a regular pattern, where the speed ramps up and down between 1000 rpm and 2000 rpm, and the load changes between 25 % and 75 % of the full load. Profile 2, which keeps the load constant at 60 % of the full load, while the speed changes with a randomly generated speed profile. Profile 3 keeps the speed constant at 1200 rpm, and then the load is randomly generated, where it repeats itself every 30 s. Stray flux measurement was collected from the PMSM operating in all mentioned profiles in the following fault condition: NF, ITSC with 5 % severity, local partial DF, and a MF case with both ITSC and DF. The DF is induced by one pole on a hot plate where two spots in the middle on one North pole have lost 30 % of original magnetic strength. The studied PMSM has 3 parallel strands, thus the severity is a estimated value of the shorted turns between the phase terminal on a single strand while the two other strands are unaffected. The ITSC is induced with a 1 Ω short circuit resistor, for mimicking the remaining insulation coating in the ITSC.

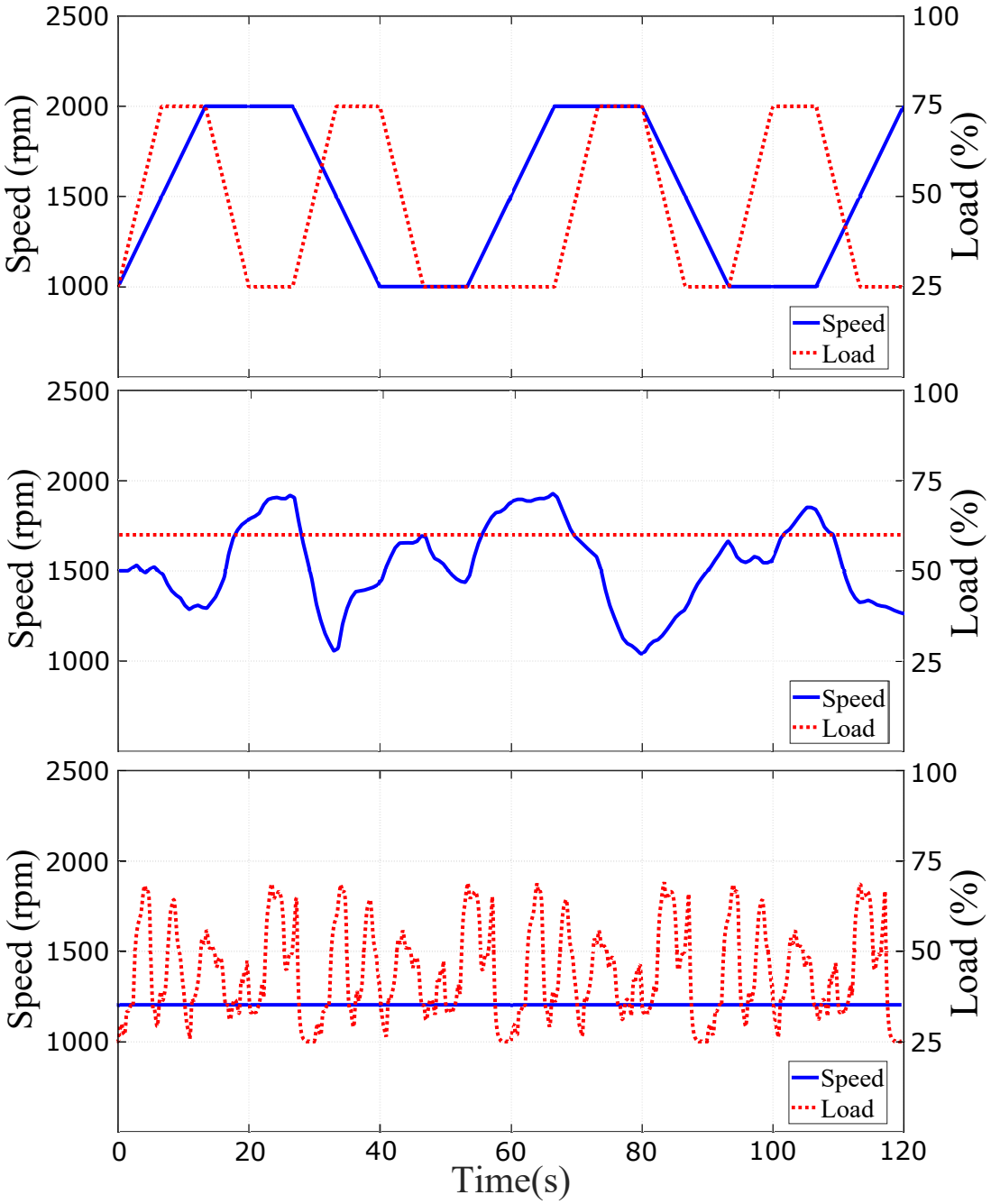

Figure F.5: The three studied operation profiles: (top) Profile 1 with variable load and variable speed, (middle) Profile 2 with constant load and variable speed, and (bottom) Profile 3 with variable load and constant speed

F.5 Results and Discussions

F.5.1 Performance of anomaly detection

The one-class SVM and LOF need to define their respected criterion for anomaly identification. The sensitivity of the one-class SVM is defined by the outlier fraction, where the portion of outliers in the training dataset is set to 10 %. The output of the trained one-class SVM under testing is a numeric score, which is less than 0 in case of an anomaly as suggested in [8]. The LOF does require trial and error to determine a suitable threshold. A value close to 1 will make the detector more sensitive but has the risk of increasing the FP rate. The threshold for LOF was set to 1.1, which means that a new point is classified as an anomaly/fault if the regions of its k^{th} nearest neighbours are on average of 10 % denser than the region of the new point. The parameter k is set to 5.

The one-class SVM and LOF classifiers are first trained on the healthy datasets from Profile 1 with the result shown in Tabel F.1 and Table F.2. The healthy dataset was split by 83.3 % (250 samples) for training and 16.7 % (50 samples) for testing. All the samples from each the faulty cases from any operation profile are used for testing (900 samples in total). Initially, the training set includes only samples from Profile 1. The performance of the one-class SVM has an accuracy of 84 % when tested on the same profile during training. The accuracy of the one-class SVM anomaly detector proposed in [8], when testing on each of the fault cases, varies between 57 % and 98.3 %. The proposed LOF algorithm, on the other hand, predicts all the fault cases as anomalies almost perfectly. However, the proposed LOF has a high FP rate. To address this issue, more samples in the healthy dataset from Profiles 2 (50 samples) and 3 (50 samples) are added to the training data to improve in the proposed FDI scheme with AL. As a result, the accuracy of the proposed LOF anomaly detector improves constantly when more samples are added. The compared one-class SVM detector suffers from the newly added data samples, where its accuracy in healthy cases improves, but FN rate increases. This proves that the proposed LOF anomaly detector could effectively identify anomalies better than the existing one when more knowledge of healthy cases is added during normal operations.

F.5.2 Training times of fault classifiers

To compare the computational effectiveness of the proposed DQN fault classifier and existing one, the average training times of DQN and the CNN benchmark are reported in Table F.3 while increasing the imbalance in datasets. The classifiers were trained with two classes (healthy and faulty), and with all four classes of healthy, DF, ITSC and MF. The training time for the DQN stays close to constant around two minutes while the training time of the CNN declines when increasing the imbalance as reported in Table F.3. The imbalance ratio λ is increased by removing samples in the faulty case. Number of steps in each of the episode in the DQN is set to 400, which would explain why the training time does not change. The CNN-based classifier on the other hand uses all available samples in each step in the training. It is noted that the imbalance of the training dataset in case of four-class is computed by the imbalance of each respected fault class. The ratio between healthy and each faulty case is considered as a more relevant metric in the compensation

Table F.1: Accuracy of one-class SVM outlier detector

Fault test case	Test	Extra samples from Profile 2 and 3					
(Criterion)	Pro.	0	50	100	150	200	250
Healthy	1	84.0	82.0	80.0	80.0	80.0	80.0
(Score $\geqslant 0$)	2	80.0	98.0	98.0	98.0	98.0	98.0
	3	46.0	70.0	80.0	80.0	84.0	90.0
DF	1	71.7	55.3	56.0	56.0	51.7	53.0
(Score < 0)	2	57.0	46.0	45.7	44.3	41.0	41.0
	3	84.0	58.3	54.7	51.0	44.7	44.3
ITSC	1	82.3	55.3	53.7	53.0	46.3	45.7
(Score < 0)	2	90.7	54.3	48.0	39.7	22.7	21.7
	3	98.3	77.0	74.7	67.0	59.0	57.0
MF	1	66.7	44.0	46.0	43.0	39.7	38.7
(Score < 0)	2	73.3	32.0	30.3	23.7	16.3	15.0
	3	93.0	62.3	58.7	51.7	42.7	37.0

Table F.2: Accuracy of LOF outlier detector

Fault test case	Test	Extra samples from Profile 2 and 3					
(Criterion)	Pro.	0	50	100	150	200	250
Healthy	1	86.0	86.0	88.0	88.0	80.0	98.0
(LOF $\leqslant 1.1$)	2	14.0	72.0	94.0	80.0	86.0	84.0
	3	8.0	52.0	88.0	80.0	82.0	90.0
DF	1	100	100	98.0	98.0	100	100
(LOF > 1.1)	2	100	98.0	100	100	100	100
	3	100	92.0	94.0	94.0	98.0	98.0
ITSC	1	100	100	100	100	100	100
(LOF > 1.1)	2	100	100	100	100	100	100
	3	100	100	100	94.0	100	100
MF	1	100	98.0	100	96.0	100	100
(LOF > 1.1)	2	100	94.0	96.0	100	100	98.0
	3	100	92.0	84.0	92.0	96.0	96.0

Table F.3: Recorded training time of DQN and CNN

Imb.	DQN		CNN	
ratio	2 classes	4 classes	2 classes	4 classes
1	133.5	125.0	279.1	525.7
1.25	131.9	123.0	233.6	437.9
1.67	132.1	120.5	209.6	348.7
2.5	131.1	122.2	187.2	284.8
5	129.4	122.0	163.2	196.4
10	129.6	124.0	140.7	155.3
15	126.5	118.4	141.1	154.9
30	127.1	119.7	142.9	139.3

described in the reward function. This study, equal imbalance (Imb.) ratios λ are applied for each fault case.

F.5.3 Performance of two-class classifiers

The proposed DQN and existing CNN fault classifiers are trained to identify a specific single fault, namely DF or ITSC. Table F.4 list the results when the DQN and the CNN classifiers are trained to identify these faults. Note, the accuracy results of the fault classifiers are listed in Table F.4, in which green-coloured numbers show the high accuracy results of over 98 % and red-coloured numbers indicate low accuracy results of less than 50 %. This is to highlight the main trends of the results. The terms of positive and negative samples will hereafter be interchangeably used with faulty and healthy case, respectively. The imbalance is increased by reducing the number of positive samples in the training dataset. All negative samples from the PMSM operating with Profile 1 are used for training, but 50 of these samples are randomly picked for testing. 50 test samples are randomly sampled from each faulty case and are sampled from the samples that are not a part of the training dataset, when $\lambda > 1$. It is noted that this selection is only applied for the testing dataset from Profile 1. All samples from Profile 2 and Profile 3 are used for testing (300 samples per class per profile). The performance of the DQN and CNN classifiers are compared with the metrics, true positive rate (TPR) and true negative rate (TNR).

In the case of DF, only the samples of the motor with an induced local demagnetisation are used as the positive training samples. The proposed DQN and existing CNN classifiers are tested on all four-fault cases, namely DF, ITSC, MF and NF or healthy, to investigate what the two other faulty datasets (ITSC and MF) can be classified. The fault signatures of MF may share common characteristics with both of DF and ITSC. Therefore, it is possible for the MF samples to be classified as a fault by the classifier trained for detecting DF or ITSC, which is why Table F.4 reports TPR for MF. Ideally, ITSC fault will not be classified as a fault by the classifiers trained for DF and vice versa. This is why Table F.4 reports TNR for the fault classifier were not trained before being used in testing.

The proposed DQN classifier and CNN achieve a TPR higher than 90 % for the fault

Table F.4: Comparing TPR and TNR of DQN and CNN classifiers when trained for identifying either DF or ITSC

		Local Demagnetisation								Inter-turn short circuit							
		DQN				CNN				DQN				CNN			
Test Pro.	Imb. ratio	TPR DF	TNR NF	TPR MF	TNR ITSC	TPR DF	TNR NF	TPR MF	TNR ITSC	TPR ITSC	TNR NF	TPR MF	TNR DF	TPR ITSC	TNR NF	TPR MF	TNR DF
1	1	100	99.9	95.8	100	97.2	98.4	73.7	99.9	98.5	97.9	12.8	99.4	95.4	96.6	2.9	99.8
	1.25	100	99.9	97.6	99.8	96.3	98.1	71.2	99.9	95.7	97.2	9.4	99.6	93.2	93.6	6.7	98.6
	1.67	100	99.7	99.6	100	95.8	98.9	71.0	100	97.1	98.1	11.5	98.8	89.1	97.9	5.8	98.8
	2.5	100	99.9	99.5	98.8	95.5	99.3	69.8	99.9	98.2	96.5	14.9	98.4	81.6	97.9	1.6	99.9
	5	100	98.7	99.6	99.1	92.9	98.6	64.3	99.9	96.4	95.6	14.7	98.9	67.6	96.9	2.1	99.8
	10	100	96.1	99.9	97.9	82.1	99.8	49.8	100	96.2	92.8	19.0	97.7	55.4	96.7	3.0	99.7
	15	99.9	93.4	99.6	95.8	69.4	97.5	35.8	99.7	93.4	90.3	15.7	98.5	43.5	99.7	2.0	99.5
	30	100	88.6	100	93.1	46.9	99.8	23.9	99.9	90.1	84.7	27.2	95.5	23.6	99.7	0.2	100
2	1	99.4	100	95.8	99.9	92.3	93.4	74.3	99.4	91.4	85.1	28.9	95.4	80.0	94.0	3.0	99.9
	1.25	99.6	99.9	97.9	100	94.8	93.7	77.1	99.5	92.7	85.1	24.6	96.6	77.8	91.0	4.8	99.7
	1.67	99.9	99.6	98.8	100	95.3	93.2	75.8	99.4	90.0	85.7	24.9	96.2	72.8	95.1	4.4	99.6
	2.5	99.8	99.1	99.5	99.7	95.2	94.8	75.9	99.4	94.6	77.9	35.1	92.3	65.0	95.9	2.0	100
	5	99.9	97.9	99.6	99.3	91.3	95.0	65.8	99.5	94.4	72.5	35.7	91.2	47.4	96.4	1.7	99.9
	10	99.9	91.6	99.8	96.4	75.4	97.5	47.3	99.9	88.0	69.9	35.1	91.7	37.6	96.3	1.4	99.8
	15	100	85.0	99.9	93.8	66.7	93.2	37.6	98.6	84.6	68.8	30.7	91.2	23.4	99.4	0.6	99.8
	30	100	72.8	100	89.8	49.1	97.6	32.2	99.3	79.6	72.3	33.2	88.0	13.2	99.5	0.3	100
3	1	97.9	99.9	89.0	100	99.0	97.1	91.6	100	82.0	91.6	12.4	99.3	76.1	94.6	5.4	99.1
	1.25	97.8	99.9	90.9	100	98.5	95.4	90.8	99.7	83.2	90.2	10.1	99.3	81.0	87.9	11.8	96.9
	1.67	98.9	99.8	94.0	99.9	99.1	96.4	93.7	100	83.8	90.1	10.9	99.3	76.9	94.6	9.4	96.6
	2.5	99.5	98.2	96.5	99.5	98.3	98.0	88.1	99.8	85.9	87.7	11.4	99.0	64.4	97.1	2.0	99.9
	5	99.6	97.0	97.5	98.9	97.5	97.6	85.9	99.8	86.6	84.8	11.4	98.8	53.9	95.3	2.0	99.8
	10	99.8	93.1	98.4	97.8	88.4	99.6	71.0	100	86.9	80.2	14.1	98.8	39.1	95.9	1.9	99.1
	15	99.7	88.4	98.4	96.3	78.0	96.3	57.2	98.6	85.2	79.0	13.3	98.2	22.5	98.4	2.6	99.0
	30	99.8	82.2	99.1	95.1	46.8	99.6	30.8	100	83.9	73.2	20.5	95.0	18.2	99.3	0.4	100

cases they are trained before testing when $\lambda = 1$. The lowest TPRs for the proposed DQN and compared CNN classifier are 82.0 % and 76.1 %, respectively when they were trained for ITSC dataset and tested on profile 3 with a constant speed and variable loads. The DQN classifier maintains a TPR of above 97.8 % when trained and tested for DF. However, the TNR for the healthy case is dropping to 72.8 %. The CNN classifier improves its TNR for the healthy case when the increasing the imbalance of the datasets . Fewer FPs is normally a positive quality in a classifier, but TPR for the CNN drops to below 50 % when increasing the imbalance in a dataset. The accuracy trend for the CNN classifier is reduced significantly when all samples are classified as healthy cases. The proposed DQN clasifier, on the other hand, reduces the possibility of FN, but has overcompensated slightly and increased FPs. Neither FP nor FN is desirable in FDI. However, both FN and FP rates can be compensated in the proposed AL scheme by correcting relabel by an expert, and the proposed DQN fault classifier has a second option with the weighted reward function.

The MF case includes both DF and ITSC. Therefore, there is a possibility that this fault case can be classified as one of those faults. This is in the context of fault classifiers, that are trained for identifying the presence of a specific fault. The test result reveals that both DQN and CNN classifiers, which are trained for DF, and it identifies MF as a fault. The TPR reported under MF is lower as compared to the case, where the classifiers are trained and tested on the same fault case. The TPR for the CNN classifier is also reduced when increasing the imbalance in datasets. Neither DQN nor CNN classifier identifies MF

as a fault when they are trained to identify ITSC fault. This result indicates that there is a high possibility that DF and MF may share the same fault signatures. The fault classifier, being trained on all four-fault cases included in this study, may find it difficult to distinguish between DF and MF.

F.5.4 Performance of four-class classifier

The proposed DQN and CNN fault classifiers are further trained with all four fault classes: DF, ITSC, MF and NF. Figure F.6 shows the hit rates of the DQN and CNN fault classifiers using test dataset in Profile 3. This includes the TNR and TPR, which were discussed in Section IV.C. The overall accuracy is also added in Figure F.6. It equals the average of the four hit rates, since the test dataset is balanced between the four classes. The proposed DQN and CNN fault classifiers suffer from being trained for all four faults. They start with an overall accuracy of 75 %, then decrease with respect to the imbalance of the dataset. Note each fault class has equal λ, which is the imbalance ratio given on the axis. The performance of the CNN is worse than the DQN, since its accuracy declines at a larger rate with a trend towards a collapse. Its hit rate for healthy case, i.e. NF, is increased towards 100 % due to this trend.

Each fault class can be incorrectly classified into three classes. This in total gives 12 miss for a four-class classifier. Figure F.7 plots the miss rates for both DQN and CNN fault classifiers, which were not close to 0. The comparison still uses the test dataset from Profile 3. It is noting that the first and last letters in the labels denote the predicted and true classes, respectively. Figure F.7a reveals that the proposed DQN fault classifier is confused between DF and MF, which were predicted in the analysis of the two-class classifiers. The DQN classifier confuses ITSC with NF and MF, while NF is generally confused with all of the other health classes. This demonstrates that the reward function may have overcompensated and needs to be adjusted. A combine decision between fault classifier and anomaly detector may also reduce the rate of FPs since Table F.2 reports a high accuracy for LOF. The CNN fault classifier does not misclassify NF with any of the fault classes. The confusion between DF and MF do decrease when increasing the imbalance, but these fault classes starts to be predicted as NF instead. Almost all samples from fault case ITSC are misclassified as NF.

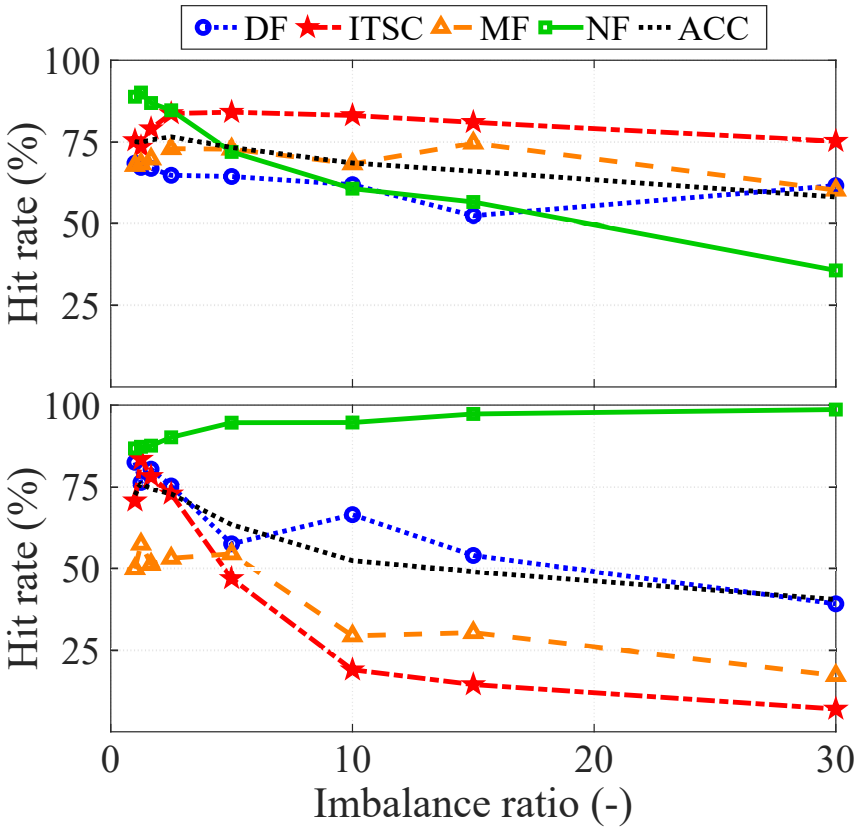

Figure F.6: Hit rates of DQN (top) and CNN (bottom) fault classifiers

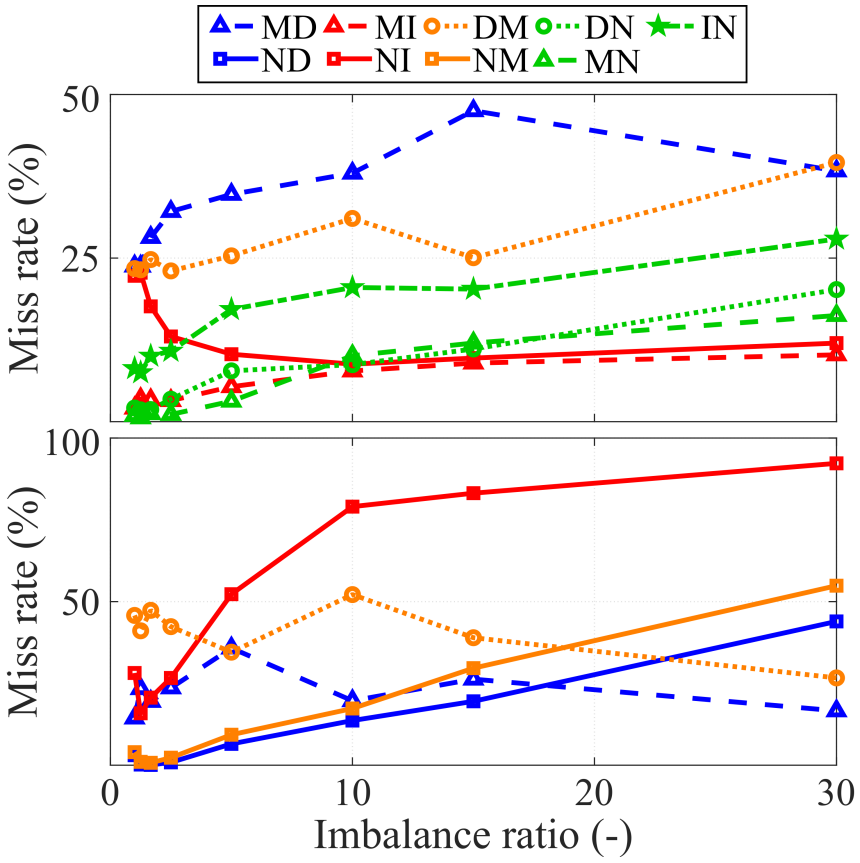

Figure F.7: Miss rates of DQN (top) and CNN (bottom) fault classifiers

F.6 Conclusion

This study proposed a fault diagnosis scheme trained and tested with both transient operating condition and mixed faults, where labelled training samples were initially unavailable. The training and testing dataset are collected by stray fluxes from the in-house test setup. The proposed method order-normalises the spectrogram by resampling the time-series data at a fixed angular increment to make it more robust against dynamic operations. The rotor position is estimated with a single external stray flux sensor, which allows for an automatic fault diagnosis of sensorless PMSM drivetrains without modifying the existing drives. The local outlier factor anomaly detector was only trained on samples from Profile 1, which gave a high false positive rate. Nevertheless, the proposed active learning framework allows for improving prediction accuracy when adding new healthy case samples. Newly discovered health classes are used to train the proposed DQN classifiers at different imbalance ratios. The comparative study shows that the DQN fault classifier is more robust than the existing CNN fault classifier, and can even have overcompensated the weight of the minority class.

References

[1] Y. Qi, E. Bostanci, V. Gurusamy, and B. Akin, "A Comprehensive Analysis of Short-Circuit Current Behavior in PMSM Interturn Short-Circuit Faults," *IEEE Transactions on Power Electronics*, vol. 33, no. 12, pp. 10 784–10 793, Dec. 2018. DOI: 10.1109/TPEL.2018.2809668.

[2] L. Wu, Y. Du, Z. Chen, Y. Guo, H. Wen, and Y. Fang, "Influence of Load Characteristics on Three-Phase Short Circuit and Demagnetization of Surface-Mounted PM Synchronous Motor," *IEEE Transactions on Industry Applications*, vol. 56, no. 3, pp. 2427–2440, Jan. 2020. DOI: 10.1109/TIA.2020.2968036.

[3] M. E. Iglesias Martínez, J. A. Antonino-Daviu, P. F. de Córdoba, J. A. Conejero, and L. Dunai, "Automatic Classification of Winding Asymmetries in Wound Rotor Induction Motors Based on Bicoherence and Fuzzy C-Means Algorithms of Stray Flux Signals," *IEEE Transactions on Industry Applications*, vol. 57, no. 6, pp. 5876–5886, Nov. 2021. DOI: 10.1109/TIA.2021.3108413.

[4] I. Zamudio-Ramirez, R. A. Osornio-Rios, J. A. Antonino-Daviu, H. Razik, and R. d. J. Romero-Troncoso, "Magnetic Flux Analysis for the Condition Monitoring of Electric Machines: A Review," *IEEE Transactions on Industrial Informatics*, vol. 18, no. 5, pp. 2895–2908, May 2022. DOI: 10.1109/TII.2021.3070581.

[5] E. A. Bhuiyan, M. M. A. Akhand, S. K. Das, and et. al., "A Survey on Fault Diagnosis and Fault Tolerant Methodologies for Permanent Magnet Synchronous Machines," *Int. J. Autom. Comput.*, vol. 17, no. 6, pp. 763–787, Nov. 2020. DOI: 10.1007/s11633-020-1250-3.

[6] Y. Qi, E. Bostanci, M. Zafarani, and B. Akin, "Severity Estimation of Interturn Short Circuit Fault for PMSM," *IEEE Transactions on Industrial Electronics*, vol. 66, no. 9, pp. 7260–7269, Sep. 2019. DOI: 10.1109/tie.2018.2879281.

[7] D. Neupane and J. Seok, "Bearing Fault Detection and Diagnosis Using Case Western Reserve University Dataset With Deep Learning Approaches: A Review," *IEEE Access*, vol. 8, pp. 93 155–93 178, Apr. 2020. DOI: 10.1109/ACCESS.2020.2990528.

[8] J. S. L. Senanayaka, H. V. Khang, and K. G. Robbersmyr, "Toward Self-Supervised Feature Learning for Online Diagnosis of Multiple Faults in Electric Powertrains," *IEEE Transactions on Industrial Informatics*, vol. 17, no. 6, pp. 3772–3781, Aug. 2021. DOI: 10.1109/TII.2020.3014422.

[9] C.-F. Tsai and W.-C. Lin, "Feature Selection and Ensemble Learning Techniques in One-Class Classifiers: An Empirical Study of Two-Class Imbalanced Datasets," *IEEE Access*, vol. 9, pp. 13 717–13 726, Jan. 2021. DOI: 10.1109/ACCESS.2021.3051969.

[10] B. Krawczyk, M. Galar, M. Woźniak, H. Bustince, and F. Herrera, "Dynamic Ensemble Selection for Multi-Class Classification with One-Class Classifiers," *Pattern Recognition*, vol. 83, pp. 34–51, Nov. 2018. DOI: 10.1016/j.patcog.2018.05.015.

[11] S. Liu, Y. Zhao, Z. Lin, *et al.*, "Data-Driven Event Detection of Power Systems Based on Unequal-Interval Reduction of PMU Data and Local Outlier Factor," *IEEE Transactions on Smart Grid*, vol. 11, no. 2, pp. 1630–1643, Mar. 2020. DOI: 10.1109/TSG.2019.2941565.

[12] T. Zhang, J. Chen, S. He, and Z. Zhou, "Prior Knowledge-Augmented Self-Supervised Feature Learning for Few-shot Intelligent Fault Diagnosis of Machines," *IEEE Transactions on Industrial Electronics*, pp. 10 573–10 584, Jan. 2022. DOI: 10.1109/TIE.2022.3140403.

[13] Y. Ding, J. Zhuang, P. Ding, and M. Jia, "Self-Supervised Pretraining via Contrast Learning for Intelligent Incipient Fault Detection of Bearings," *Reliability Engineering and System Safety*, vol. 218, p. 108 126, Feb. 2022. DOI: https://doi.org/10.1016/j.ress.2021.108126.

[14] C. Huang, "Featured Anomaly Detection Methods and Applications," Doctor of Philosophy in Computer Science, University of Exeter, 2018, pp. 115–124. [Online]. Available: https://ore.exeter.ac.uk/repository/%20bitstream/handle/10871/34351/HuangC.pdf?sequence=1.

[15] M. Chen, K. Zhu, R. Wang, and D. Niyato, "Active Learning-Based Fault Diagnosis in Self-Organizing Cellular Networks," *IEEE Communications Letters*, vol. 24, no. 8, pp. 1734–1737, Aug. 2020. DOI: 10.1109/LCOMM.2020.2991449.

[16] Y. Lu, Y.-M. Cheung, and Y. Y. Tang, "Bayes Imbalance Impact Index: A Measure of Class Imbalanced Data Set for Classification Problem," *IEEE Transactions on Neural Networks and Learning Systems*, vol. 31, no. 9, pp. 3525–3539, Nov. 2020. DOI: 10.1109/TNNLS.2019.2944962.

[17] R. Razavi-Far, M. Farajzadeh-Zanjani, and M. Saif, "An Integrated Class-Imbalanced Learning Scheme for Diagnosing Bearing Defects in Induction Motors," *IEEE Transactions on Industrial Informatics*, vol. 13, no. 6, pp. 2758–2769, Sep. 2017. DOI: 10.1109/TII.2017.2755064.

[18] M. E. Khoda, T. Imam, J. Kamruzzaman, I. Gondal, and A. Rahman, "Robust Malware Defense in Industrial IoT Applications Using Machine Learning with Selective Adversarial Samples," *IEEE Transactions on Industry Applications*, vol. 56, no. 4, pp. 4415–4424, Aug. 2020. DOI: 10.1109/TIA.2019.2958530.

[19] B. Jang, M. Kim, G. Harerimana, and J. W. Kim, "Q-Learning Algorithms: A Comprehensive Classification and Applications," *IEEE Access*, vol. 7, pp. 133 653–133 667, Sep. 2019. DOI: 10.1109/access.2019.2941229.

[20] Z. Song, J. Yang, X. Mei, T. Tao, and M. Xu, "Deep Reinforcement Learning for Permanent Magnet Synchronous Motor Speed Control Systems," *Neural Computing and Applications*, vol. 33, no. 10, pp. 5409–5418, May 2021. DOI: 10.1007/s00521-020-05352-1.

[21] L. Wen, X. Li, and L. Gao, "A New Reinforcement Learning Based Learning Rate Scheduler for Convolutional Neural Network in Fault Classification," *IEEE Transactions on Industrial Electronics*, vol. 68, no. 12, pp. 12 890–12 900, Dec. 2021. DOI: 10.1109/tie.2020.3044808.

[22] E. Lin, Q. Chen, and X. Qi, "Deep Reinforcement Learning for Imbalanced Classification," *Applied Intelligence*, vol. 50, no. 8, pp. 2488–2502, Mar. 2020. DOI: 10.1007/s10489-020-01637-z.

[23] Y. Zhang, Z. Zhang, Q. Yang, D. An, D. Li, and C. Li, "EV Charging Bidding by Multi-DQN Reinforcement Learning in Electricity Auction Market," *Neurocomputing*, vol. 397, pp. 404–414, Jul. 2020. DOI: https://doi.org/10.1016/j.neucom.2019.08.106.